BACHELOR

# Film damage by photons, ions and radicals during plasma-enhanced atomic layer deposition

Smits, M.

*Award date:*
2019

Technische Universiteit
Eindhoven
University of Technology

Department of Applied Physics
Plasma & Materials Processing group

# Film damage by photons, ions and radicals during plasma-enhanced atomic layer deposition

*Bachelor Thesis*

M.Smits (0966699)

Supervisors:
ir. K.Arts
dr.ir. H.C.M Knoops

Eindhoven, February 2019

# Abstract

In this project plasma damage caused by photons, ions and radicals during plasma atomic layer deposition (ALD) is investigated for two different materials: passivated silicon and graphene. This is done to gain an insight in which plasma species causes damage to what sort of material. The outcome of the measurements on passivated silicon is that radicals and ions do not cause a significant decrease in charge carrier lifetime. Therefore vacuum ultra violet (VUV) photons are responsible for the decrease in charge carrier lifetime of passivated silicon. The outcome of the measurements on graphene is that graphene is transparent for the in this experiment used amount of VUV photons. In contrast, both radicals and ions are responsible for the degradation of graphene. Combining these results, it can thus be concluded that both ions and radicals can only cause surface damage during plasma ALD processes, because of their limited penetration depth. In contrast, VUV photons can cause more damage in the bulk, because of their larger penetration depth.

# Contents

# Abbreviations

| | |
|---|---|
| ALD | Atomic layer deposition |
| VUV | Vacuum ultra violet |
| Ar | Argon |
| $O_2$ | Oxygen |
| $Al_2O_3$ | Aluminium Oxide |
| $MgF_2$ | Magnesium Fluoride |
| DMAI | Dimethylaluminium isoproxide |
| TMA | Trimethylaluminium |
| SRH | Shockley-Read-Hall |
| CVD | Chemical vapour deposition |
| PEALD | Plasma-enhanced atomic layer depostion |
| ICP | Inductively coupled plasma |

# Chapter 1

# Introduction

In this section the goals of this project are described. Also an insight is given in why this research is done and the main research questions of this project are formulated.

## 1.1 Electronics in daily life

Nowadays nano-electronics are used in almost every electronic device, whether it is a smartphone, airplane or home appliances. These electronics are used to make life easier and more comfortable, for example more computational power to computers or giving memory and more options to home appliances. The computational power of a chip scales with the number of transistors on that chip. Intel co-founder Gordon Moore stated that the number of transistors on a chip can be doubled every two years[32]. To maintain Moores law, each transistor must be scaled down. Therefore atomic scale processing techniques are needed to guarantee atomic precision and a good working device. A key example of such a technique is atomic layer deposition(ALD). This technique is already used in some key steps for synthesis of atomically thin films with precise thickness control.
Another field in which ALD can play an important role is the deposition of passivation layers on solar cells. Solar energy is a renewable energy which emits almost no greenhouse gasses and plays therefore an important role in future energy supply. To maximize the efficiency of a solar cell, a passivation layer is grown on top of a semiconductor material which confines the charge carriers inside the device and limits recombination.

## 1.2 Atomic layer deposition

As mentioned in section 1.1, ALD is an important deposition technique for the growth of materials on the atomic scale. In most cases a (silicon) substrate is placed in a reactor and is exposed to a precursor. This precursor reacts with the reactive groups on the substrate as shown in figure 1.1a.This first step is self-limiting because each surface group can only bind one precursor atom. When all reactive groups have reacted with the precursor molecules, the chamber is purged. This means that all precursor molecules and reaction products are removed from the reactor chamber as shown in figure 1.1b. In case of thermal ALD the third step is to add a reactant to the chamber, for example water vapour to grow oxides. This water binds to the atom indicated in blue in figure 1.1c. This step is also self-limiting and when all molecules have reacted, the chamber is purged. The result after one cycle is shown in figure 1.1d. In case of plasma-enhanced atomic layer deposition (PEALD) the reactant is replaced by a plasma. If these cycles are repeated in this way and the reactants are inserted sufficient time in the reactor to let all the reactants react, a uniform layer of the desired material will form on top of the substrate.

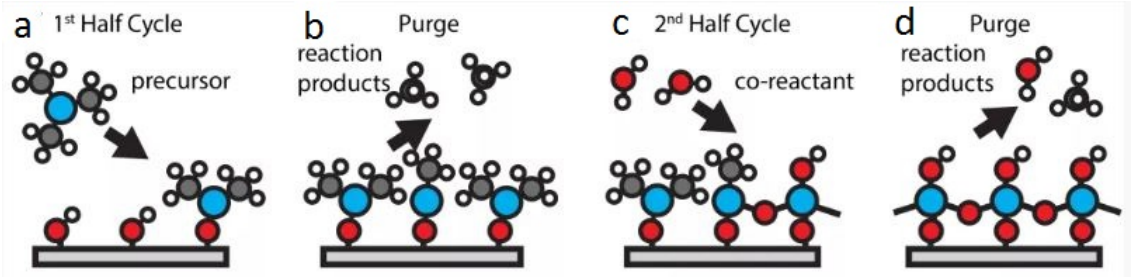


Figure 1.1: Different steps in ALD cycle. In the first step a precursor is added to the chamber, the second step is purging the chamber, the third step is adding a reactant to the chamber and the fourth step is purging the chamber again[31].

## 1.3 Plasma ALD

Plasma is besides solid, liquid and gas the fourth phase of a substance. In solid, liquid and gas phase an electron cloud is bounded to an atom core due to coulomb interaction. If energy is added to a system to disrupt this coulomb interaction(e.g. by an electric field), atoms can ionize into a positively charged nucleus and negatively charged electrons. These electrons can cause a chain reaction by ionizing other atoms and molecules. When a significant amount of atoms are ionized and the properties of the substance are changed(e.g. electric conductivity), a substance is in plasma phase. Besides ionizing an atom, which results in an ion, an electron can break up chemical bounds between atoms. In case of an oxygen plasma this results in oxygen radicals. This is useful because radicals have an unpaired electron and are therefore highly reactive[25]. These radicals are important in an ALD process. Because of their high reactivity, short cycle times can be achieved. Another property of a plasma is it non-thermal equilibrium. This means that electrons often have temperatures of several eV, while heavier particles like ions and radicals are still close to room temperature. This allows for low temperature depositions, which is a major advantage because if a device is heated before a deposition process, it can loose important device properties [5, 25]. There are more benefits of plasma ALD over thermal ALD. Plasma properties can be controlled by, e.g., pressure, power and gas flow, giving a high flexibility in process conditions. It is reported that for some materials, plasma assisted ALD leads to better film density, better electronic properties and less impurities[11, 14, 13]. In thermal ALD, oxides are deposited with $H_2O$ as reactant. Some precursors are non or low reactive with $H_2O$. Plasma species can be more reactive with these precursors[25, 22]. Besides more material choices, it is reported for plasma ALD to have a higher growth per cycle in some cases[21].

Besides all advantages of plasma ALD there are some problems which can be present during plasma ALD. A plasma contains many different species which can all cause damage to materials[27]. Species that can cause damage are:

1. Vacuum Ultra Violet(VUV) photons
2. Ions
3. Radicals

Each of these species can cause different type of damage as will be discussed in section 2.1[15]. VUV photons can penetrate deep into a material and will therefore cause more electronic defects in the bulk[15]. In contrast, high energetic ions and radicals have limited pentration depth and causes more structural damage on a surface of a material[24]. During this project the damage caused in the bulk of a material is investigated with passivated silicon, while the damage caused on a surface is investigated with graphene.

## 1.4 This project

To investigate the damage caused by different species in a plasma, the properties of two materials are investigated after a certain plasma exposure time. It is hard to distinguish the damage caused by different species because they are all present at the same time in a plasma. However ions and radicals can be blocked using a magnesium fluoride window which transmits the VUV with wavelength larger than 115 nm. In this project, the damage on passivated silicon and graphene is characterized. The measurements on passivated silicon can be compared with the results that are found by Profijt *et al*[24]. The main question of this project is:

**How are films damaged due to photons, ions and radicals during plasma ALD?**

Relevant questions that are answered during this project are:

1. Which plasma species cause damage on a 20 nm thick $Al_2O_3$ passivation layer on silicon?
2. Which plasma species cause damage on a single layer of graphene?
3. What is the difference between damage caused by an argon or oxygen plasma?

First, in section 2, the theoretical background of damage mechanisms of different plasma species and material properties that indicates plasma damage will be discussed. In section 3 the used diagnostics and plasma systems are discussed, further the experimental method is explained. In section 4 the results are presented, after the results are presented and discussed. From these results several conclusions can be made, which is given in section 5.

# Chapter 2

# Theory

## 2.1 Plasma damage

Plasma damage is a well known phenomenon, but it is hard to distinguish the damage caused from different species. In this section, the properties of different plasma species are discussed.

### 2.1.1 Vacuum Ultra Violet photons

VUV photons are photons which can due to their high energy only propagate in vacuum, under atmospheric conditions they are absorbed within centimeters. To ionize a molecule or atom, electrons are pumped to higher energy bands. Instead of ionizing an atom an electron can relax from a high energy level to the ground level by emitting a photon[8]. The energy of the emitted photons only depends on the difference between two energy levels.

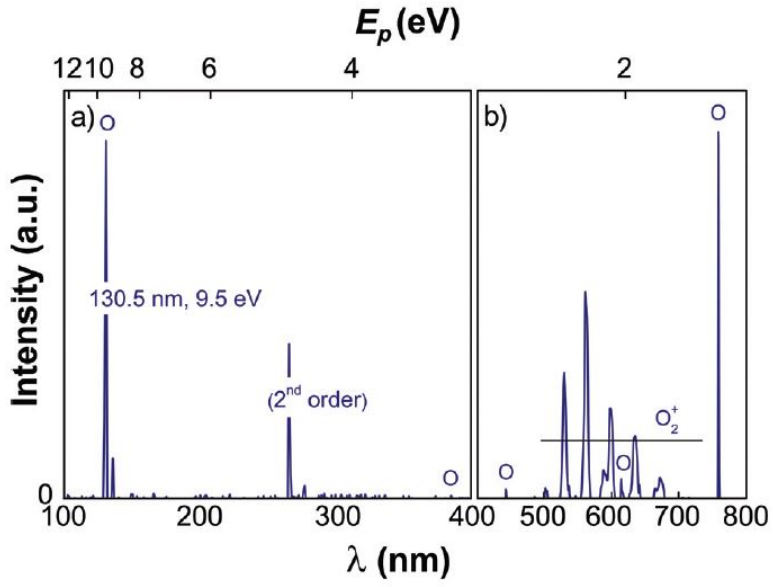


Figure 2.1: Graph that shows the emission spectrum of an oxygen plasma with corresponding wavelength and energy. In part a) the VUV spectrum is shown which contains wavelenghts from 100-200 nm and energies from 8-12 eV. In part b) the visible spectrum is shown[24].

In figure 2.1 the emission spectrum of an oxygen plasma is shown. Dependent on the material in which the VUV photons are absorbed, the VUV photons can often penetrate deep into a material

and cause damage. For instance when a dielectric is grown on top of a semiconductor, a photon can photoinject electrons from the semiconductor material to the dielectric on top [16]. In this work, the damage caused by photons is investigated by monitoring the carrier lifetime of $Al_2O_3$ passivation layers. A passivation layer prevents charge carrier to recombine at the surface. This can be achieved in several ways, reducing the recombination at the interface (chemical passivation) or shielding charge carriers inside the device by an electric field(field-effect passivation). Both passivation properties can be damaged due to VUV photons[17].

Field effect passivation is confining the wanted charge carrier inside the silicon device[17]. This is done by a charge density in the passivation layer, which repels charge carriers from the interface[17]. An incoming photon can photo-emit charge carriers out of this layer which causes a decrease in charge density. This can lead to poorer field-effect passivation as the electric field is dependent on the net charge difference[16].

Chemical passivation is preventing charge preventing charge carriers to recombine through defects[3]. Defects in the bulk can be minimized, but at the edges, defects will always be present because each silicon atom has one unpaired electron at the edge of the crystal lattice. If it remains unpaired it forms a dangling bond and this dangling bond can form an electronic accessible state. If this state is close to the center of the bandgap of the semiconductor, it forms a good spot for Schokley-Read-Hall recombination which is explained in section2.2.1. If the silicon atoms at the edge are passivated with other atoms, such as hydrogen, these electronic accessible states are removed. This is beneficial for the efficiency of the solar cell because it minimizes recombination. High energetic photons can create these interfacial defects and therefore more recombination will take place, which is undesirable for the efficiency of the solar cell [3].

### 2.1.2 Ions

Another specie that is present in a plasma are ions. Ions are charged particles and the ions arriving at the substrate have higher energy than the ions in the plasma center. This is because they are accelerated to the substrate. This acceleration region is formed because electrons have higher thermal velocity than ions. Due to this velocity difference, a net charge difference will be formed between the substrate and plasma center. To maintain zero net current, an electric field is induced which accelerates the ions towards the substrate. The potential difference between the plasma and substrate can be expressed as below in (2.1).

$$V_p - V_f = \frac{T_e}{2e} + \frac{T_e}{2e} \ln \frac{m_i}{2m_e\pi}, \tag{2.1}$$

where $V_p$is plasma potential $V_f$ is substrate potential $T_e$ is electron energy in $eV$ and $m_i$ and $m_e$ the ion and electron mass. Typically this difference is a few multiples of the electron energy. The ions will be accelerated by this electric field and will gain energy until they collide with the substrate. The ion energy is $E_{ion} = e(V_p - V_f)$ where e is the electron charge.

The interaction between ion and surface depends on the energy and mass of the incoming ions and can be divided into three regimes:

1. Single-knockon regime 2.2a
2. Lineair cascade regime2.2b
3. Spike regime 2.2c

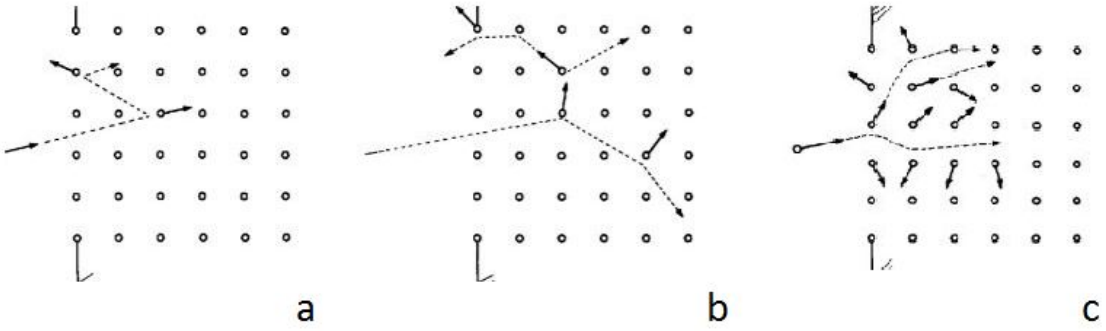


Figure 2.2: Different sputtering methods where (a) is single-knockon regime, (b) is lineair cascade regime and (c) is the spike regime. The regimes are ordered from low to high ion energy[28].

In the single-knockon regime the energy of the ion is transferred to an atom which is emitted from the grid, if the transferred energy is larger than the binding energy. There is almost no movement of other atoms in the grid. In the lineair cascade regime the energy is higher and causes more movement deep in the atom grid. In the spike regime the incoming ion-energy is high enough to dislocate atoms in a large region called the spike region. In this region vacancies will appear and the lattice is therefore more damaged [28]. In a typical $O_2$ plasma the ion energy is around 30 eV [24]. This ion energy corresponds a penetration depth of roughly 1 nm in silicon[10]. Therefore on a 15-25 nm thick $Al_2O_3$ passivation layer, the impact from ions is expected to mainly cause surface damage.

### 2.1.3 Radicals

Besides photons and ions there are radicals present in a plasma. Radicals are highly reactive particles because of an unpaired electron. Therefore they are very useful in plasma ALD to react with the precursor and achieve short plasma times. But because of the high concentration of radicals in a plasma and their high reactivity, they can also cause undesired reactions on materials[1]. Because of the high reactivity they can remove or displace double bounds in aromatic materials like graphene[18]. Oxygen radicals can also cause impurities while depositing materials, i.e., oxygen impurities while depositing $HfN_x$[12]. The damage caused by radicals is also dependent on material properties. It can cause for instance more damage on 2D materials than 3D materials, because of limited penetration depth during plasma exposure.

## 2.2 Parameters that indicates plasma damage

To investigate the influence of plasma exposure on different materials, the quality and properties of the material need to be determined. In this project two different materials are investigated, both have other properties. In this section the quality parameters of the two different materials are discussed.

### 2.2.1 Carrier lifetime

The quality of the passivation layer of a solar cell depends on the charge carrier lifetime. Charge carrier lifetime is the average time before an electron hole pair recombines. This is an undesired process in a solar cell, because when charge carriers recombine, they cannot contribute to the net current of the solar cell. To prevent carriers from recombination, it is good to know what processes can occur within a solar cell. Four different recombination processes can occur that influence the effective lifetime[29]:

1. Radiative recombination

2. Auger recombination
3. Shockley-Read-Hall (SRH) recombination
4. Surface recombination

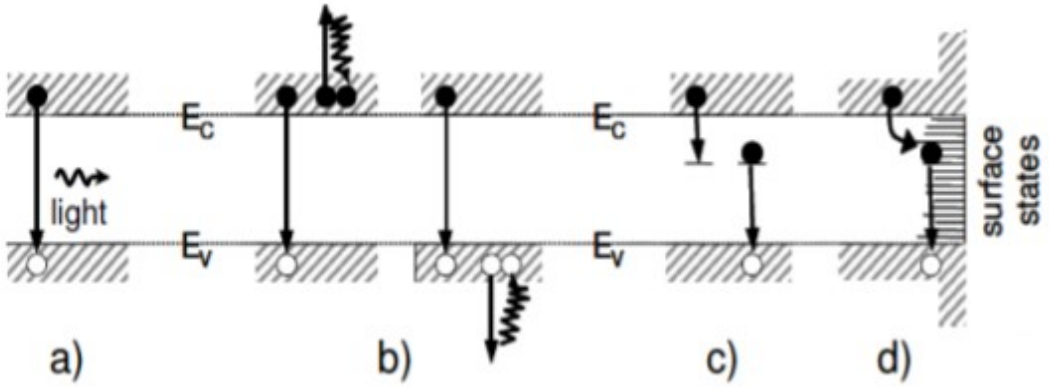


Figure 2.3: Different recombination processes, where a) displays radiative recombination, b) displays auger recombination, c) displays Schockley-Read-Hall recombination and d) displays surface recombination[29].

In radiative recombination an electron in the conduction band recombines with a hole in the valence band while emitting a photon with an energy of approximately the bandgap energy as shown in figure 2.3a. This is the dominating recombination process within a direct bandgap semiconductor. Nowadays most solar cells are made of silicon which has an indirect bandgap and therefore radiative recombination in a silicon solar cell is negligible. Auger recombination, which is shown in figure 2.3b involves three charge carriers, where also an electron from the conduction band recombines with a hole in the valence band. Instead of emitting energy as a photon, the energy is transferred to a hole in the valence band or electron in the conduction band. After this gain in energy the particle loses energy due to phonons until it is at the edge of the band again. When there are many excess carriers, Auger recombination is the dominating process. The third mechanism is SRH recombination that is shown in figure 2.3c. This process contains two steps, first a charge carrier moves to a region which is formed by defects or doping and emit a photon or multiple phonons. If the charge carrier moves to the valence or conduction band before it relaxes back to its desirable band, it will recombine with a charge carrier from the other band and emit the energy in form of a photon. This process is most likely when the energy level is somewhere in the middle between the conduction and valence band, else the electron is often re-emitted into the conduction band. At the solar cell surface, the crystal lattice will be ended and will contain many defects. All these defects have accessible regions for charge carriers, therefore the recombination rate at the surface is high as shown in figure 2.3d. The effective charge carrier lifetime depends on all separate recombination times as shown in (2.2)[29].

$$\frac{1}{\tau_{eff}} = \frac{1}{\tau_{rad}} + \frac{1}{\tau_{Auger}} + \frac{1}{\tau_{SRH,bulk}} + \frac{1}{\tau_{Surface}} \tag{2.2}$$

Most recombination processes can be minimized by avoiding defects by passivating the solar cell. Only Auger recombination cannot be prevented[26]. So if the passivation layer is practically perfect, Auger recombination is the limiting factor for the effectivity of a silicon solar cell [24]. After plasma exposure the passivation layer of the solar cell can be damaged by one of the species that are present in a plasma.

### 2.2.2 Raman spectrum

Graphene is a 2D hexagonal lattice that consists of carbon atoms. Because it is a two dimensional lattice, the vibrational modes are very sensitive for impurities in the lattice. With Raman spectroscopy these vibrational modes can be detected. Raman spectroscopy is a popular method to investigate structural properties of a material. The material is irradiated with a single wavelength laser. The photons scatter on the sample and the scattered photons are detected by the detector. Some photons are scattered elastically and have therefore the same energy as before the scatter process. Other photons scatter inelastically and when they are detected by the detector, an energy difference is observed. This difference corresponds to a vibrational mode of the material. The Raman shift of these bands can be calculated with formula (2.3)[2].

$$R_{shift}\left(cm^{-1}\right) = \left(\frac{1}{\lambda_0} - \frac{1}{\lambda_1}\right) \cdot 10^7, \tag{2.3}$$

where $R_{shift}$ is Raman shift in $cm^{-1}$, $\lambda_0$ in nm the excitation wavelength of the laser and $\lambda_1$ in nm the wavelength of the Raman scattered photon. A photon can scatter on the material in three different processes:

1. Rayleigh scattering
2. Stokes Raman scattering
3. Anti-Stokes Raman scattering.

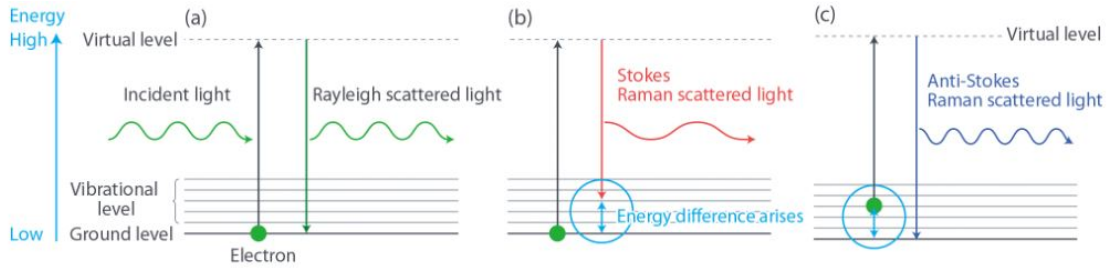


Figure 2.4: Different scattering processes, displayed from energy level to energy level, where (a) displays Rayleigh scattering, (b) displays Stokes Raman scattering and (c) displays Anti-Stokes Raman scattering[19].

When a photon scatters elastically, it will only distort an electron cloud, called Rayleigh scattering. When a photon scatters inelastically, the photon transfers energy to the material or the material transfers energy to the photon which corresponds to Stokes Raman scattering and Anti-Stokes Raman scattering, respectively. The three different processes are shown in figure 2.4. As discussed in section 3.1.2, the Raman spectrum of graphene is used to investigate structural damage of the graphene after plasma exposure.

# Chapter 3

# Experimental setup

## 3.1 Diagnostics

Diagnostics are used to measure the charge carrier lifetime of passivated silicon and the Raman spectrum of graphene. In this section the working of the used diagnostics is discussed.

### 3.1.1 Lifetime measurements on passivated silicon

In this project the charge carrier lifetime measurements are done with a Photoconductance Lifetime Tester WCT-120 from Sinton instruments. A schematic overview of this instrument is shown in figure 3.1.

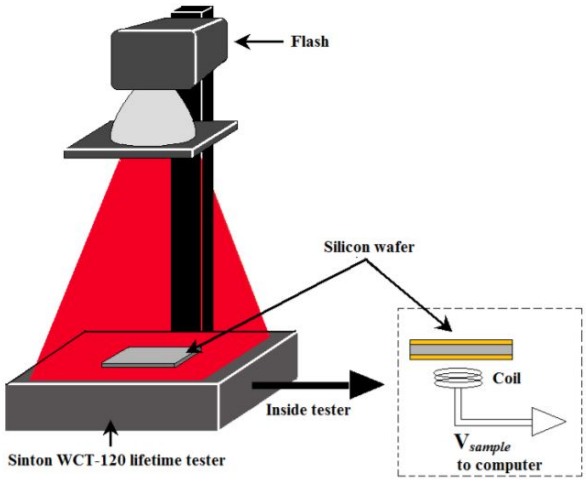


Figure 3.1: Schematic overwiew of a Photoconductance Lifetime Tester WCT-120 from Sinton instruments[9]

A light flash generates excess carriers in a silicon wafer, leading to an increase in conductance in the wafer. This causes an increase in magnetic field, which is detected by the coil under the sample due to inductivity. The lifetime can be measured in three different modes:

1. Transient
2. Quasi steady state
3. Generalized

To maintain consistency all measurements are done in generalized mode. The generalized mode is the most accurate mode for determining the lifetime between 50 and 200 $\mu$s and in this project the samples will be degraded to low lifetimes. Still, it must be checked that the illumination time of the sample is not too long or short at longer lifetimes. This mode uses equation (3.1)[9]

$$\tau_{Eff} = \frac{\Delta n(t)}{G - \frac{d\Delta n}{dt}}, \tag{3.1}$$

where $\tau_{Eff}$ denotes the effective lifetime, $\Delta n$ the carrier density and G the carrier generation in the sample. This equation is only valid for a surface recombination velocity less then 100 cm/s,[9] Which is the case for silicon wafers which were used during this project. To remain accurate charge carrier lifetimes, the samples must be larger than the coil under the sample.

### 3.1.2 Raman spectroscopy on Graphene

As mentioned in section 2.2.2, Raman spectroscopy is used to find the structural properties of a material. In this project the Raman spectroscopy measurements are done with an Invia Raman Microscope of Renishaw. The 50x objective is used and all measurements are done with a laser of wavelength 512 nm with 1 % intensity. The peaks that indicate graphene are the so called G- and 2D band. [20] When graphene is damaged, for example by plasma exposure, the intensity of the graphene peaks will degrade and the intensity of the D peak will increase. The Raman spectrum for typical and damaged graphene is shown in figure 3.2.

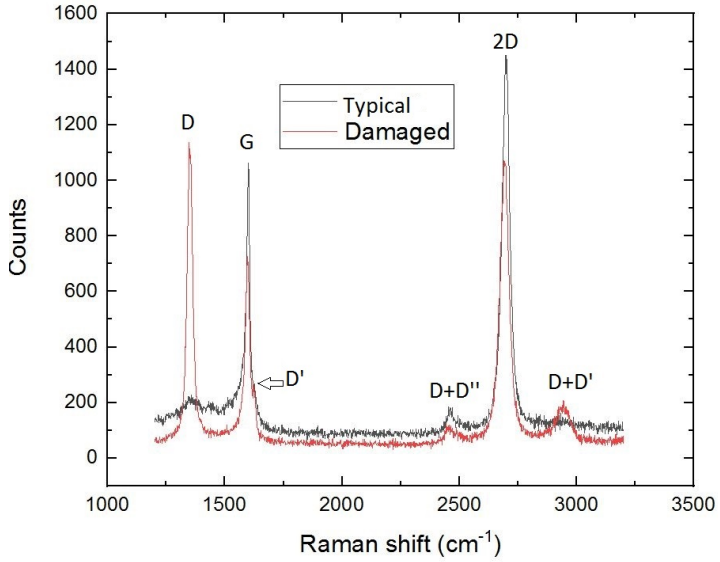


Figure 3.2: Raman spectrum for typical(black) and damaged(red) graphene. For typical graphene, the G peak and 2D peak are dominant. When the graphene is damaged or less pure the D peak will rise and the G peak will decrease. The ratio of heights between the D an G peak gives information about the defect ratio.

The D band is indicative for the amount of defects in the graphene layer. The ratio between the D and G peak will give information about the defect ratio ($n_d$) in the graphene sample as stated in equation (3.2). Here the height of the peaks can be taken as intensity $I$ [7].

$$n_d \propto \sqrt{\frac{I(D)}{I(G)}} \tag{3.2}$$

What stands out from figure 3.2 is the broad signal around 1600 $cm^{-1}$, this indicates amorphous carbon. To maintain accurate defect ratios, this peak, if present, is also taken into account.

## 3.2 Plasma systems

In this section the used plasma systems are discussed. The FlexAL2 reactor is often used for plasma-enhanced ALD, the Kaleidos reactor is a new reactor and the properties of this reactor are tested during this project.

### 3.2.1 FlexAL2

The FlexAL2 reactor of Oxford Instruments is located in the NanoLab@TU/e and is used to expose graphene and passivated silicon samples with argon and oxygen plasmas. It is a PEALD reactor, but no ALD processes are done during this project. The plasma is generated with an inductively coupled plasma source (ICP-source), which is located in a chamber just above the reactor vessel. The system contains a loadlock which can operate circular wafers up to 200 mm in diameter. In this project only small samples of graphene and aluminiumoxide passivation layers on silicon are used. The used reactor is shown in figure 3.3.

Figure 3.3: Picture of Oxford instruments plasma ALD system (FlexAL2) which is located in Nanolab@Tu/e [30]

The conditions (pressure, power and gasflow) can be varied. The used conditions are given in table 3.1. FlexAL allows running processes where the plasma can be turned on and off for specific times. Kaleidos, that is discussed in section 3.2.2 does not have this option.

### 3.2.2 Kaleidos

Kaleidos is a new plasma reactor which operates at different conditions than FlexAL2. The operating conditions are shown in table 3.1. The plasma source in Kaleidos is different from the ICP-source that is used in FlexAL2. Moreover the plasma in Kaleidos is generated closer to the sample which would suggest that more plasma species reach the sample. However, the standard pressure is higher in Kaleidos, which lowers the concentration of plasma species in the reactor. The timing of plasma exposure in Kaleidos is done with a stopwatch, for short exposures this is not as accurate as in FlexAL2.

Table 3.1: Reactor conditions used during this project. Only one gas is used at the time so no mixtures.

| Plasma system | Pressure (mTorr) | Gas flow (sccm) | Power (W) |
|---|---|---|---|
| Flexal 2 | 50-75 | 100(oxygen) or 100(argon) | 100 |
| Kaleidos | 410-415 | 80(oxygen) or 85(argon) | 50 |

## 3.3 Method

In this section an insight is given in what experiments are done to attain the measurements results. The section is divided into two subsections, one for each material. After the approach is explained, the validation of the plan is investigated.

### 3.3.1 Passivated silicon

The $Al_2O_3$ passivation layers of the samples used in this work were grown under different conditions. The growth conditions of the samples are shown in table 3.2, all wafers are n-type.

Table 3.2: Growth conditions of $Al_2O_3$ passivation layers grown on n-type silicon wafers. The samples are ordered with letters. The thickness of all passivation layers is approximately 20 nm. Two different precursors are used: Trimethylaluminium(TMA) and Dimethylaluminum isopropoxide (DMAI). The anneal process is done with a rapid thermal anneal device (RTA). The samples are annealed with a nitrogen gas for 10 minutes.

| Sample | Plasma/Thermal ALD | Precursor | T growth (°C) | T anneal (°C) |
|---|---|---|---|---|
| A,B and C | Plasma | TMA | 200 | 400 |
| D | Thermal | DMAI | 200 | - |
| E | Thermal | DMAI | 300 | - |

First the charge carrier lifetime, before plasma exposure, of each passivated silicon sample is determined with the Sinton lifetime measurer. Each time the lifetime is measured three times, these are averaged to minimize the error. To distinguish which plasma species cause damage, one sample is covered with a circular Magnesium Fluoride window with a thickness of five millimeter and a diameter of one inch. This window will block the ions and radicals and transmits VUV photons with a wavelength higher than 115 nm as shown in figure 3.4. For an $O_2$ plasma, this corresponds to 60-70 % transmission for the VUV peak around 130 nm, which was also used to correct the transmission by Harald *et al*[24]. This sample is placed into a reactor with another sample without window. After the samples are placed in the reactor, they are exposed to an oxygen plasma for a certain time. After the plasma exposure, the charge carrier lifetime of the samples will again be determined with the Sinton lifetime measurer. Repeating this step for different exposure times will relate the degradation of the samples with plasma exposure time. The damage can be caused by only VUV photons, radicals and ions. To distinguish the damage caused by radicals or ions, another sample is placed into a reactor and is now exposed with an argon plasma, which contains no radicals.

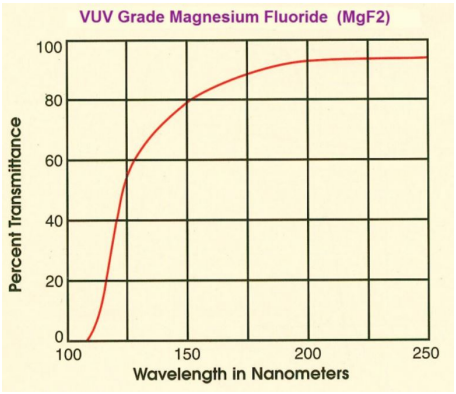


Figure 3.4: Transmission graph of a Magnesium Fluoride window in the VUV wavelength range[6]. Note that this transmission graph does not originate from the manufacturer of the used window. Therefore a rough estimation of the transmission is taken.

### 3.3.2 Graphene

In this work 1 $cm^2$ CVD-grown graphene is used, which has been transferred to a silicon substrate with a polymethylmethacrylate supporting layer as described by Vervuurt *et al*[31].

First the defect ratio is determined with a Raman spectroscope, 10 different spots are taken and averaged to minimize the effect of spatial dependency. Then again two samples are placed into a reactor, one with and one withouth the $MgF_2$ window. The samples are exposed with an oxygen plasma for a certain time, after the exposure the defect ratio is again determined. Repeating this step will relate the degrading of the samples with plasma exposure time. To distinguish the damage caused by radicals or ions, another sample is placed into a reactor and is now exposed with an argon plasma, which contains no radicals. To compare the two plasma systems as discussed in section 3.2, the experiments are done in both reactors.

### 3.3.3 Validation of lifetime measurement

As mentioned in section 3.1.1 the passivated silicon samples must be larger than the coil of the Sinton Lifetime Tester. This means that during the measurements on passivated silicon not the whole sample is covered by the 1 inch diameter Magnesium Fluoride window. To identify the effect of the non-covered part on the decrease in lifetime, one sample is covered with a quartz window of the same size as the Magnesium Fluoride window. The quartz window blocks all plasma species. Both the covered sample and non-covered sample are placed into the reactor and are exposed to an oxygen plasma for two minutes. After the exposure the charge carrier lifetime is measured. The result is shown in table 3.3

Table 3.3: Table with the normalized charge carrier lifetime before and after plasma exposure. One sample is partly covered with a quartz window that blocks all species. Another sample is exposed to all plasma species.

| Plasma exposure time (s) | Lifetime with quartz window | Lifetime without quartz window |
|---|---|---|
| 0 | 1 | 1 |
| 120 | 0,79 | 0,28 |

In table 3.3, the decrease in lifetime after plasma exposure is shown. The edge effects of the uncovered part of the sample with quartz window are relatively low compared to the non-covered sample. Therefore, if the sample that is covered with a $MgF_2$ window shows a similar decay

in lifetime as the non-covered sample, this decay mostly corresponds to VUV radiation rather than edge effects. Therefore the experiment with the Magnesium Fluoride window is relevant to determine what species causes damage on different materials.

# Chapter 4

# Results & Discussion

## 4.1 Passivated silicium

In this section the results of the experiments on aluminiumoxide passivation layers on silicon are presented and discussed. The growth conditions of the used samples are shown in table 3.2. All results on passivated silicon are obtained with FlexAL2.

First an uncovered sample indicated with A in table3.2 is used to relate the plasma exposure time and charge carrier lifetime. This exposure is done with an oxygen plasma(100 sccm, 50mTorr, 100 W, FlexAL2). The result is plotted in figure 4.1, where the charge carrier lifetime is plotted on logarithmic scale because an exponential relation is expected from Profijt *et al.* [24].

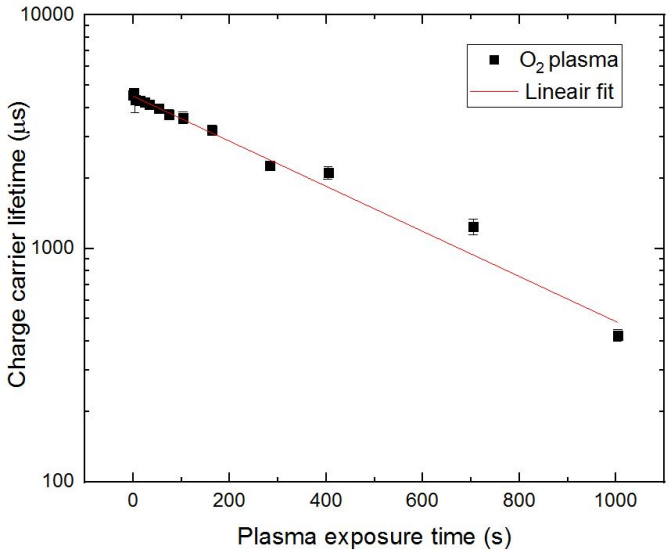


Figure 4.1: Measured charge carrier lifetime as function of cumulative oxygen plasma exposure time (100 sccm, 50mTorr, 100 W, FlexAL2, sample A). The charge carrier lifetime is plotted on logarithmic scale and the date is fitted with a lineair fit indicated in red.

As expected, the lifetime is decreasing as function of cumulative plasma exposure time. This decrease can be caused by all plasma species that are discussed in section 2. The relation in figure 4.1 seems to be exponential and is therefore fitted with a lineair fit on the logarithmic scale. The fit parameter of the fit is the slope, which is -9,66·$10^{-4}$/s. From the slope, the decay time can be calculated with $Slope = -1/t_{decay}$, where the decay time indicates the plasma exposure time

corresponding to a decrease in charge carrier lifetime to 10% of its initial value. The decay time is 1035 s. This corresponds to a decay in charge carrier lifetime from 4500 $\mu$s to 450 $\mu$s. This can also be checked with figure 4.1.

To distinguish the damage caused between VUV photons or radicals and ions, two other samples are placed into the reactor, one with Magnesium Fluoride window and one without any coverage. The charge carrier lifetimes after plasma exposure time is shown in figure 4.2. The lifetimes are normalized to make a comparison between the two samples.

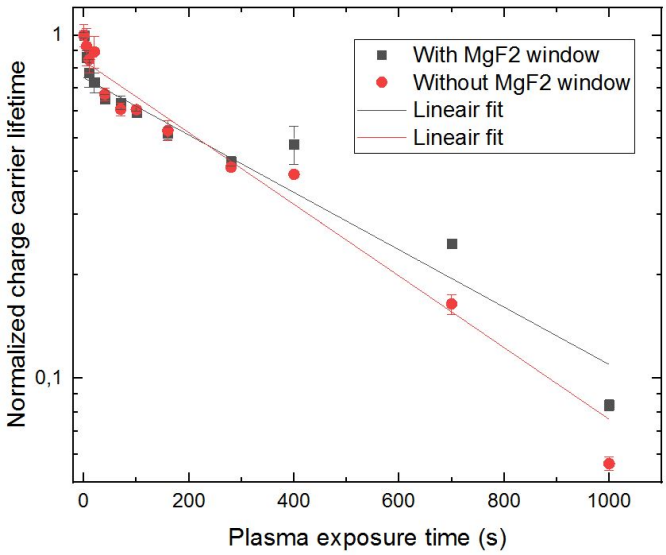


Figure 4.2: Measured normalized charge carrier lifetime as function of cumulative oxygen plasma exposure time(100 sccm, 50mTorr, 100 W, FlexAL2, samples B and C). The normalized charge carrier lifetime is plotted on logarithmic scale. The grey points indicates the sample (B) with Magnesium Fluoride window. The red points indicates the sample (C) without any coverage. The data are fitted with lineair fits.

In figure 4.2 it can be seen that the normalized charge carrier lifetime decreases as function of cumulative plasma exposure time. The decrease in lifetime of the two different samples is similar. This suggests that the damage is caused by only the VUV photons, because all radicals and ions are blocked and VUV photons are mostly transmitted by the Magnesium Fluoride window. What stands out is that the line indicated in black is less steep than the line indicated in red. This is expected because the transmission of the Magnesium Fluoride window is 60 % and therefore less VUV photons reach the sample. The decay times can be calculated with the slope. This gives for the samples with and without window respectively 1198 and 962 s. To correct for the 60-70 % transmission of the Magnesium Fluoride window, the decay time of the sample with window must be multiplied by 0.65, which gives 779 s. The error in the decay times is around 10 %, which lead to decay times in the range of 1080-1320(covered), 866-1058(uncovered) and 700-857(covered corrected). This is a little bit smaller than the decay time of the non-covered sample. This might be due to the effect of the exposed edges as is discussed in section 3.3.3.

In figures 4.1 and 4.2, some of the measurements are done at a temperature of 200 °C, other measurements are done at 50 °C. To determine the effect of the high temperature exposures, a damaged sample is placed into the reactor for 10 minutes at 200 °C. Hereafter the sample is annealed with a rapid thermal anneal(RTA) device for 10 minutes at 400 °C. The corresponding bar chart is shown in figure 4.3.

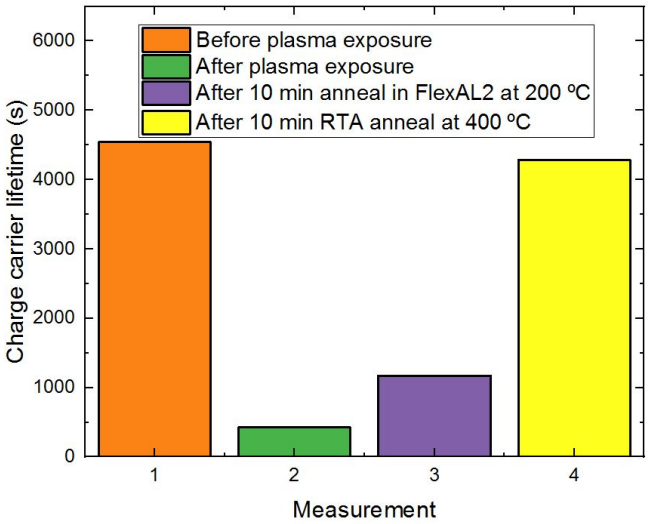


Figure 4.3: Charge carrier lifetimes plotted at different moments of the experiment. The orange bar is the lifetime of the unexposed sample. The green bar is the lifetime of the fully degraded sample. The purple bar indicates the lifetime of the sample after it is heated for 10 minutes at 200 °C in the reactor. The yellow bar indicates the charge carrier lifetime after the sample is annealed for 10 minutes with a rapid thermal anneal (RTA) device at 400 ° C.

As expected, the charge carrier lifetime of the sample before any plasma exposure is high. During the experiment the charge carrier lifetime is decreased in various plasma exposure steps untill it is around 10% of the initial value. The influence of the high temperature in the reactor is visible, the lifetime increased with 150% of its value before the heating experiment. After the RTA anneal, the charge carrier lifetime is approaching its initial value to around 95%. This confirms the idea that some damage is counteracted when the measurements done at 200°C. This can explain why some points in figures 4.1 and 4.2 are above the trend line.

Samples D and E are grown with precursor DMAI instead of TMA. The lifetimes of these samples are already decreased to one-tenth of theirs initial values after 10-20 seconds plasma exposure. The reason for this fast decrease is not determined in this project, but it could be related to the structure of the film and interface[23].

## 4.2 Graphene

In this section the results of the experiments on graphene are discussed. First the results obtained with FlexAL2 are presented and secondly the results obtained with Kaleidos are presented. At last a comparison between the two different reactors is given.

To distinguish the damage caused by VUV photons or radicals and ions, two samples are placed into the reactor. One sample is fully covered with a Magnesium Fluoride window, that will block the ions, radicals and 30-40 % of the VUV photons, the other sample is uncovered. Then the samples are exposed to an oxygen plasma, after which the Raman spectrum is measured again. The obtained results are shown in figure 4.4.

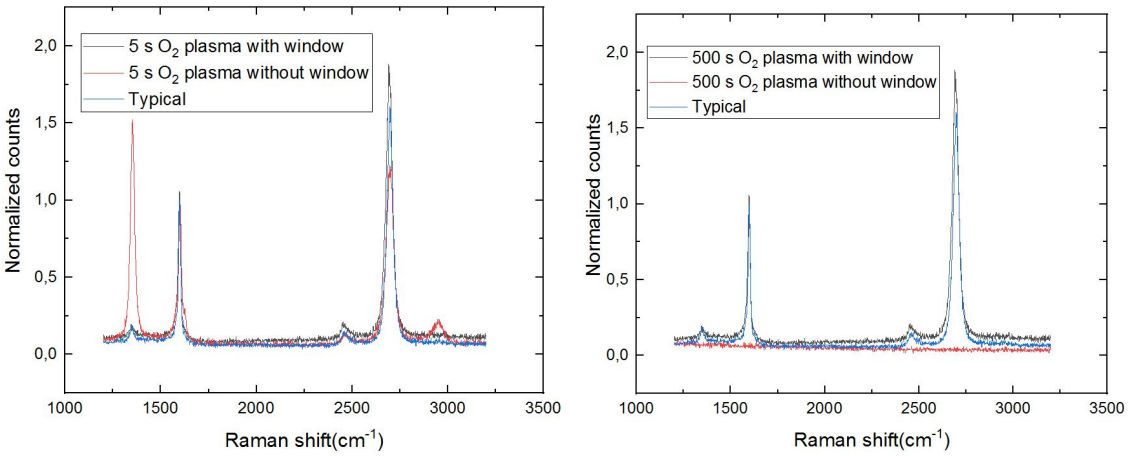


Figure 4.4: Raman spectra after 5(a) and 500(b) s $O_2$ plasma exposure(100 sccm, 50mTorr, 100 W, FlexAL2). For a good view on the ratio between the D and G peak, the spectra are normalized on the G peak. The red line indicates the sample without window. The blue line indicates typical graphene and the grey line indicates the sample with Magnesium Fluoride window.

In figure 4.4, the Raman spectra after 5(figure 4.4a) and 500(figure 4.4b) seconds plasma exposure are shown. What stands out from both figures is that the Raman spectrum of the covered sample is not changing during the whole experiment. In contrast, the D peak of the uncovered sample is increased drastically after 5 seconds $O_2$ plasma exposure and the Raman spectrum is even on the whole domain after 500 seconds plasma exposure. This means that the graphene is completely etched away from the substrate due to the plasma exposure. Because the Magnesium Fluoride window transmits 60-70 % of the incoming VUV photons of an $O_2$ plasma, and that sample remains undamaged, this experiment proves that during a plasma ALD process under these conditions, the flux of VUV photons is insufficient to cause significant damage on the graphene substrate. Therefore the damage on graphene is only caused by radicals and/or ions. This indicates that radicals and ions causes surface damage during plasma ALD. This surface damage can be minimized by first growing a few nanometer with thermal ALD.

To distinguish the damage caused by radicals and ions, another sample is exposed to an argon plasma. Argon is an atomic noble gas and an argon plasma does not contain radicals. In figure 4.5, the defect ratio is plotted as function of plasma exposure time. Because of the local differences in the graphene samples, the defect ratios of 10 points are averaged for a more accurate defect ratio.

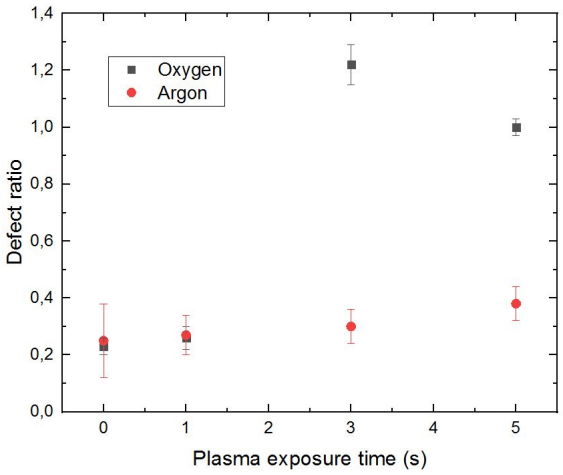


Figure 4.5: Defect ratio (D/G peak ratio of Raman spectrum) plotted as function of plasma exposure time (100 sccm, 50mTorr, 100 W, FlexAL2) for short exposure times. Red indicates a sample exposed to an argon plasma and gray indicates the sample exposed to an oxygen plasma.

From figure 4.5 it is clear that an oxygen plasma causes more damage on a graphene sample than an argon plasma. What stands out is that after the first plasma exposure step of one second, the defect ratios are more or less the same. But when this exposure step is extended to two seconds a big difference is observed. This difference might result from a certain striking time before the plasma is really on and therefore the exposure was in reality not 1 s.The defect ratio of the sample that is exposed to oxygen seems to decrease in the last exposure step, while the defect ratio of the sample exposed to argon increases slightly. Based on the D/D$'$ ratios, it is likely that the $sp^3$ defects are created first, and the vacancy defects are created while etching away the graphene[4]. As a consequence of this etching, the Raman spectrum contains only noise as is shown in 4.4. Therefore at a certain point the ratio between the D and G peak will not be representative for the damage anymore.

From figure 4.5 it becomes clear that oxygen radicals and oxygen ions, present in an $O_2$ plasma cause more damage on graphene than argon ions present in an argon plasma. To compare the two plasma systems, the argon measurement is continued in FlexAL2, while a new argon measurement is started in Kaleidos. The results of this measurement series are shown in figure 4.6. Note that, per particle, the oxygen ions might cause more damage than oxygen radicals. This can be determined in future work by shielding the ions from the substrate. If the obtained damage is similar to a sample exposed to ions an radicals, the damage is caused mainly by the radicals.

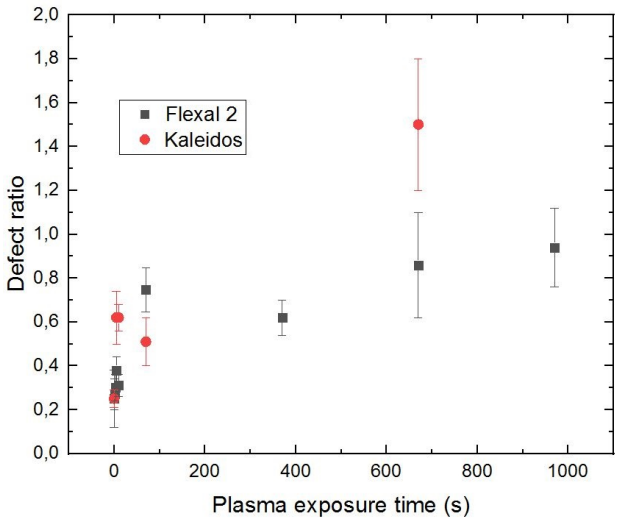


Figure 4.6: Defect ratio plotted as function of argon plasma exposure time, for the two different plasma systems. Red is Kaleidos and grey is FlexAL2. This graph indicates long plasma exposure times compared to figure4.5. The reactor conditions are shown in table 3.1

.

In figure 4.6 the defect ratio as function of plasma exposure time is plotted, for Kaleidos in red and FlexAL2 in black. A sample that is exposed to an argon plasma reaches a defect ratio of around 1.2 after more than ten minutes of plasma exposure. In contrast, a sample that is exposed to an oxygen plasma reach this value already after three seconds, as shown in figure 4.5. This indicates that an oxygen plasma, containing reactive radicals causes the most damage on a graphene sample. It is hard to make a comparison between the results obtained with Kaleidos and FlexAL2 because the defect ratio develops in the same way in both plasma systems. The error is high because the defect ratio stongly depends on the chosen spot. This local dependency of the samples can have a significant influence on the result. Therefore no hard statements can be made on the comparison between FlexAL2 and Kaleidos, except that for short plasma exposure times (<50 s) moderate damage is found and for long plasma exposure times (>500 s) high damage is found for both plasma systems.

# Chapter 5

# Conclusions

In this project, the influence of different plasma species during an plasma ALD process is investigated. The investigated species are: VUV photons, ions and radicals. There are some useful results obtained, which give rise for new questions and experiments. These are discussed in chapter 6. The main conclusions of this project are discussed below.

## 5.1 Passivated silicon

By performing the carrier lifetime measurements on 18-22 nm thick $Al_2O_3$ passivation layers on silicon, different conclusions can be made. Firstly it is demonstrated that because of the limited penetration depth, ions and radicals do not cause a significant decrease in charge carrier lifetime of passivated silicon samples. This is concluded because the sample that is exposed to all species shows a similar decay as the sample that is exposed to only VUV photons. The decay must therefore be caused by the VUV photons emitted by a plasma. These can penetrate deep into the passivation layer, while ions and radicals only penetrate 1-3 nm into the layer. It is shown that if samples are annealed after plasma exposure, their charge carrier lifetime can almost fully be restored.

## 5.2 Graphene

By performing Raman measurements on a graphene sample, the properties of the graphene sample can be determined. Based on these measurements different conclusions are made. Firstly it is demonstrated that the amount of VUV photons emitted by an oxygen plasma is not enough to induce damage on a graphene sample. Secondly, the damage caused by argon ions compared with oxygen radicals and ions for short plasma exposure times is very small. This indicates that radicals cause more damage than ions, but this can not be said with 100 % certainty as oxygen ions can also cause more damage than argon ions. To support this statement other experiments can be done. These experiments are discussed in chapter 6.

# Chapter 6

# Future research

## 6.1 Passivated silicon

Due to size limitations of the passivated silicon samples, the samples were not covered completely. A larger Magnesium Fluoride window is ordered, but not delivered in time of the project. When the window is delivered new measurements on passivated silicon can be done to achieve consistent results between the uncovered and covered sample.

## 6.2 Graphene

To distinguish the damage caused by oxygen radicals and ions and argon ions, the ions can be shielded from the sample with a charged grid. Secondly, it is tried to linearize the data from argon and oxygen plasma exposure. Relations with the in table 3.1 shown conditions are found for argon and oxygen and are respectively plasma exposure time$^{0.25}$(figure6.1) and plasma exposure time$^{4}$. For a oxygen plasma it is hard to determinate the relation because really short exposure times are needed. For argon it can be verified with different samples under different conditions.

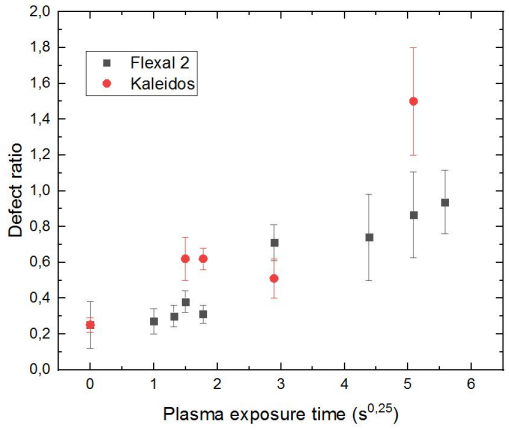


Figure 6.1: Defect ratio (D/G peak ratio of Raman spectrum) plotted as function of plasma exposure time$^{0,25}$ (100 sccm, 50mTorr, 100 W, FlexAL2) for long exposure times.

# Acknowledgments

For the last three months i worked at the PMP group. To do a research has been interesting and it was a great experience to work individually in the cleanroom.

I would like to thank Karsten for his supervision and tips on how to do a research or write a report. I learned a lot, from thinking about the next step in an experiment to analyzing data and think about how do you present found results. I also want to thank Harm Knoops for revising my report and help me with presenting results.

Furthermore, I want to thank Christian for the explanation of the Raman spectroscope and help when FlexAL2 was down. I want to thank Willem-jan for his explanation of the Sinton lifetime measurer and RTA device. I want to thank Roel for the passivated silicon samples and Nando for the cleanroom tour. Lastly the technicians of the PMP group for the labtour and labacces.

# Bibliography


[1] H. V. Bui, F. Grillo, and J. R. V. Ommen. Atomic and molecular layer deposition : off the beaten track. *Chemical Communications*, 53:45–71, 2016. ISSN 1359-7345. doi: 10.1039/C6CC05568K. URL http://dx.doi.org/10.1039/C6CC05568K. 6

[2] C.Otto. URL https://www.utwente.nl/en/tnw/mcbp/documentation/fundamentals/raman.pdf. 8

[3] G. Dingemans. No Title. page 227, 2011. 5

[4] A. Eckmann, A. Felten, A. Mishchenko, L. Britnell, R. Krupke, K. S. Novoselov, and C. Casiraghi. Probing the nature of defects in graphene by Raman spectroscopy. *Nano Letters*, 12(8):3925–3930, 2012. ISSN 15306984. doi: 10.1021/nl300901a. 19

[5] K.-E. Elers, J. Winkler, K. Weeks, and S. Marcus. TiCl[sub 4] as a Precursor in the TiN Deposition by ALD and PEALD. *Journal of The Electrochemical Society*, 152(8):G589, 2005. ISSN 00134651. doi: 10.1149/1.1938108. URL http://jes.ecsdl.org/cgi/doi/10.1149/1.1938108. 2

[6] Esourceoptics. URL http://www.esourceoptics.com/vuv_material_properties.html. 13

[7] A. C. Ferrari and D. M. Basko. Raman spectroscopy as a versatile tool for studying the properties of graphene. *Nature Nanotechnology*, 8(4):235–246, 2013. ISSN 17483395. doi: 10.1038/nnano.2013.46. 10

[8] A. M. Fox. *An introduction Quantum optics*. Oxford university press, Oxford, 6 edition, 2014. ISBN 978-0-19-856673-01. 4

[9] N. E. Grant. Surface passivation and characterisation of crystalline silicon by wet chemical treatments. (December), 2012. 9, 10

[10] D. B. Graves and D. Humbird. Surface chemistry associated with plasma etching processes. 192(2002):72–87, 2009. 6

[11] B. Hoex, J. Schmidt, P. Pohl, M. C. Van De Sanden, and W. M. Kessels. Silicon surface passivation by atomic layer deposited Al2O3. *Journal of Applied Physics*, 104(4), 2008. ISSN 00218979. doi: 10.1063/1.2963707. 2

[12] S. Karwal, B. L. Williams, J. Niemelä, M. A. Verheijen, W. M. M. Kessels, and M. Creatore. Plasma-assisted atomic layer deposition of HfNx : tailoring the film properties by the plasma gas composition. (2017), 2019. doi: 10.1116/1.4972208. URL http://dx.doi.org/10.1116/1.4972208. 6

[13] J. H. Kim, D. S. Kil, S. J. Yeom, J. S. Roh, N. J. Kwak, and J. W. Kim. Modified atomic layer deposition of Ru O2 thin films for capacitor electrodes. *Applied Physics Letters*, 91(5):1–4, 2007. ISSN 00036951. doi: 10.1063/1.2767769. 2

[14] M.-S. Kim, S. A. Rogers, Y.-S. Kim, J.-H. Lee, and H.-K. Kang. Atomic layer deposition analysis of HfSiO_4 by mass spectroscopy and XPS. *J. Electrochem. Soc.*, 45(5):1317–1321, 2004. ISSN 03744884. 2

[15] H. C. Knoops, S. E. Potts, A. A. Bol, and W. M. Kessels. *Atomic Layer Deposition*, volume 3. Elsevier B.V., second edi edition, 2014. ISBN 9780444633057. doi: 10.1016/B978-0-444-63304-0.00027-5. URL http://dx.doi.org/10.1016/B978-0-444-63304-0.00027-5. 2

[16] J. L. Lauer, J. L. Shohet, and R. W. Hansen. Measuring vacuum ultraviolet radiation-induced damage. *Journal of Vacuum Science & Technology A: Vacuum, Surfaces, and Films*, 21(4):1253–1259, 2003. ISSN 0734-2101. doi: 10.1116/1.1565152. URL http://avs.scitation.org/doi/10.1116/1.1565152. 5

[17] S.-s. Letters. Influence of the oxidant on the chemical and field-effect passivation of Si by ALD Al2O3 Influence of the Oxidant on the Chemical and Field-Effect Passivation of Si by ALD Al 2 O 3. (2011):3–7, 2019. doi: 10.1149/1.3501970. 5

[18] P. K. Maurya, F. Radical, R. O. Species, and F. Reagent. derstand and Fight Aging Animal Biotechnology as a Tool to Un- Learn more about Hydroxyl radical Hydroxyl radical. 6

[19] nanophoton. URL https://www.nanophoton.net/raman/raman-spectroscopy.html. 8

[20] D. Němeček and G. J. Thomas. Raman Spectroscopy of Viruses and Viral Proteins. *Frontiers of Molecular Spectroscopy*, pages 553–595, 2009. ISSN 1626183392. doi: 10.1016/B978-0-444-53175-9.00016-7. 10

[21] S. J. Park, W. H. Kim, H. B. R. Lee, W. J. Maeng, and H. Kim. Thermal and plasma enhanced atomic layer deposition ruthenium and electrical characterization as a metal electrode. *Microelectronic Engineering*, 85(1):39–44, 2008. ISSN 01679317. doi: 10.1016/j.mee.2007.01.239. 2

[22] S. E. Potts, L. Schmalz, M. Fenker, B. Diaz, J. Swiatowska, V. Maurice, A. Seyeux, P. Marcus, G. Radnoczi, L. Toth, and W. M. M. Kessels. Ultra-Thin Aluminium Oxide Films Deposited by Plasma-Enhanced Atomic Layer Deposition for Corrosion Protection. *Journal of The Electrochemical Society*, 158(5):C132, 2011. ISSN 00134651. doi: 10.1149/1.3560197. URL http://jes.ecsdl.org/cgi/doi/10.1149/1.3560197. 2

[23] S. E. Potts, G. Dingemans, and C. Lachaud. Plasma-enhanced and thermal atomic layer deposition of Al 2 O 3 using aluminum precursor. 2(2):1–12, 2012. doi: 10.1116/1.3683057. 17

[24] H. B. Profijt, P. Kudlacek, M. C. M. van de Sanden, and W. M. M. Kessels. Ion and Photon Surface Interaction during Remote Plasma ALD of Metal Oxides. *Journal of The Electrochemical Society*, 158(4):G88, 2011. ISSN 00134651. doi: 10.1149/1.3552663. URL http://jes.ecsdl.org/cgi/doi/10.1149/1.3552663. 2, 3, 4, 6, 7, 12, 15

[25] H. B. Profijt, S. E. Potts, M. C. M. van de Sanden, and W. M. M. Kessels. Plasma-Assisted Atomic Layer Deposition: Basics, Opportunities, and Challenges. *Journal of Vacuum Science & Technology A: Vacuum, Surfaces, and Films*, 29(5):050801, 2011. ISSN 0734-2101. doi: 10.1116/1.3609974. URL http://avs.scitation.org/doi/10.1116/1.3609974. 2

[26] A. Richter, S. W. Glunz, F. Werner, J. Schmidt, and A. Cuevas. Improved quantitative description of Auger recombination in crystalline silicon. *Physical Review B - Condensed Matter and Materials Physics*, 86(16):1–14, 2012. ISSN 10980121. doi: 10.1103/PhysRevB.86.165202. 7

[27] H. Shi, D. Shamiryan, J. F. de Marneffe, H. Huang, P. S. Ho, and M. R. Baklanov. *Plasma Processing of Low-k Dielectrics*. Number October 2017. 2012. ISBN 9780470662540. doi: 10.1002/9781119963677.ch3. 2

[28] P. Sigmund. *Sputtering by ion bombardment : Theoretical concepts 2 . Sputtering by Ion Bombardment : Theoretical Concepts*. Number January 1981. 2017. ISBN 3540105212. doi: 10.1007/3540105212. 6

[29] L. Tous. *Nickel/Copper Plated Contacts as an Alternative to Silver Screen Printing for the Front Side Metallization of Industrial High Efficiency Silicon Solar Cells*. Number January 2014. 2014. ISBN 9789460187889. 6, 7

[30] TUE. Oxford instruments flexal2. URL https://www.tue.nl/en/research/research-institutes/research-institutes/nanolabtue/list-of-equipment/ald-equipment/oxford-instruments-flexal-2/. 11

[31] R. H. Vervuurt, W. M. Kessels, and A. A. Bol. Atomic Layer Deposition for Graphene Device Integration. *Advanced Materials Interfaces*, 4(18):1–19, 2017. ISSN 21967350. doi: 10.1002/admi.201700232. 2, 13

[32] M. Waldrop. More then Moore. *Nature*, 530(11. February):145, 2016. ISSN 0028-0836. doi: 10.1038/530144a. 1